Monthly Notices of the ROYAL ASTRONOMICAL SOCIETY

MNRAS **471,** L96–L100 (2017) doi:10.1093/mnrasl/slx097
Advance Access publication 2017 July 27

The relation between stellar magnetic field geometry and chromospheric activity cycles – I. The highly variable field of ϵ Eridani at activity minimum

S. V. Jeffers,[1★] S. Boro Saikia,[1] J. R. Barnes,[2] P. Petit,[3,4] S. C. Marsden,[5] M. M. Jardine,[6] A. A. Vidotto[7] and the BCool collaboration

[1]*Institut für Astrophysik, Georg-August-Universität, Friedrich-Hund-Platz 1, D-37077 Göttingen, Germany*
[2]*School of Physical Sciences, The Open University, Walton Hall, Milton Keynes MK7 6AA, UK*
[3]*UPS-OMP, Institut de Recherche en Astrophysique et Planétologie, Université de Toulouse, F-31400 Toulouse, France*
[4]*Institut de Recherche en Astrophysique et Planétologie, 14 Avenue Edouard Belin, F-31400 Toulouse, France*
[5]*Computational Engineering and Science Research Centre, University of Southern Queensland, Toowoomba 4350, Australia*
[6]*SUPA, School of Physics and Astronomy, University of St Andrews, North Haugh, St Andrews, Fife KY 16 9SS, UK*
[7]*School of Physics, Trinity College Dublin, the University of Dublin, Dublin-2, Ireland*

Accepted 2017 June 13. Received 2017 June 2; in original form 2016 December 14

ABSTRACT

The young and magnetically active K dwarf ϵ Eridani exhibits a chromospheric activity cycle of about 3 yr. Previous reconstructions of its large-scale magnetic field show strong variations at yearly epochs. To understand how ϵ Eridani's large-scale magnetic field geometry evolves over its activity cycle, we focus on high-cadence observations spanning 5 months at its activity minimum. Over this time-span, we reconstruct three maps of ϵ Eridani's large-scale magnetic field using the tomographic technique of Zeeman–Doppler imaging. The results show that at the minimum of its cycle, ϵ Eridani's large-scale field is more complex than the simple dipolar structure of the Sun and 61 Cyg A at minimum. Additionally, we observe a surprisingly rapid regeneration of a strong axisymmetric toroidal field as ϵ Eridani emerges from its S-index activity minimum. Our results show that all stars do not exhibit the same field geometry as the Sun, and this will be an important constraint for the dynamo models of active solar-type stars.

Key words: techniques: polarimetric – stars: activity – stars: individual: ϵ Eridani – stars: magnetic field – stars: solar-type.

1 INTRODUCTION

The evolution of the Sun's large-scale magnetic field ranges from dipolar at activity minimum to complex at activity maximum (DeRosa, Brun & Hoeksema 2012). A solar-like magnetic cycle has also been observed in the K dwarf 61 Cyg A, where its large-scale field is a simple dipole at activity minimum. In this Letter, we investigate the evolution of the large-scale magnetic field of ϵ Eridani, which is well established to be a magnetically active star (Valenti, Marcy & Basri 1995; Metcalfe et al. 2013). Previously in Jeffers et al. (2014), we reconstructed the large-scale magnetic field geometry of ϵ Eridani to understand how the photospheric large-scale magnetic field geometry of ϵ Eridani varies over its S-index cycle. These observations comprise six epochs spanning nearly 7 yr or approximately two S-index cycles. We showed that each map has evolved dramatically from one epoch to the next, and that we clearly reconstruct the weakest magnetic field structures at its Ca II H&K (or S-index) minimum. The motivation for this work is to investigate the evolution of ϵ Eridani's large-scale magnetic field with a higher cadence of observations over its S-index minimum to understand how its field evolution differs from the Sun and 61 Cyg A. To achieve this, we obtained spectropolarimetric observations every night, weather permitting, over a period of 5 months.

2 OBSERVATIONS AND DATA ANALYSIS

We observed ϵ Eridani over a time-span of 5 months from 2014 September to 2015 January using the high-resolution spectropolarimeter NARVAL located at the Telescope Bernard Lyot, France (Aurière 2003). The total data set comprises 40 spectra that were obtained every night with acceptable observational conditions and are summarized in Table 1 (shown later). The data were reduced and processed following an identical procedure already explained in section 3 of Jeffers et al. (2014).

All Stokes *I* and Stokes *V* reduced spectra were processed using least-squares deconvolution (LSD; Donati et al. 1997). By extracting the information contained in each spectral line, LSD enables the

★ E-mail: jeffers@astro.physik.uni-goettingen.de

Table 1. Journal of observations. Phase = 0 is defined as Julian Date = 245 4101.5 and is used for all epochs, with subsequent epochs taking phase = 0 as an integer number of rotational periods from this value. The exposure time of all observations is 400 s.

Date	Julian Date (+245 4000)	UT	Phase	LSD S/N	S-index
		Map 1 (2014.71)			
2014 September 1	2902.67	04:05:45	−1.1737	39 478	0.402
2014 September 2	2903.68	04:24:48	−1.0870	36 435	0.396
2014 September 3	2904.67	04:00:01	−1.0029	37 224	0.395
2014 September 5	2906.65	03:38:55	−0.8329	42 847	0.394
2014 September 11	2912.65	03:33:12	−0.3195	35 636	0.404
2014 September 12	2913.62	02:53:49	−0.2362	38 801	0.399
2014 September 13	2914.66	03:47:37	−0.1474	39 293	0.396
2014 September 23	2924.64	03:16:40	0.7069	38 855	0.405
2014 September 24	2925.6	02:19:16	0.7891	36 714	0.396
2014 September 25	2926.62	02:52:49	0.8767	35 734	0.403
2014 September 27	2928.61	02:36:02	1.0469	35 976	0.391
		Map 2 (2014.84)			
2014 October 16	2947.65	03:36:25	−1.3227	30 832	0.396
2014 October 17	2948.49	23:49:35	−1.2506	34 626	0.395
2014 October 18	2949.63	03:09:04	−1.1531	36 745	0.392
2014 October 19	2950.58	01:59:09	−1.0717	28 518	0.393
2014 October 24	2955.48	23:37:39	−0.6520	29 839	0.405
2014 October 25	2956.56	01:23:13	−0.5601	36 520	0.403
2014 October 26	2957.44	22:40:33	−0.4842	24 285	0.410
2014 October 28	2959.59	02:07:25	−0.3006	33 182	0.402
2014 October 29	2960.53	00:47:06	−0.2198	36 670	0.401
2014 October 30	2961.49	23:39:16	−0.1382	33 682	0.397
2014 October 31	2962.51	00:13:05	−0.0506	36 824	0.401
2014 November 1	2963.51	00:10:47	0.0349	42 832	0.403
2014 November 12	2974.53	00:45:23	−1.0213	20 765	0.388
2014 November 15	2977.48	23:38:01	−0.7684	31 998	0.309
2014 November 20	2982.45	22:45:26	−0.3435	21 015	0.387
		Map 3 (2014.98)			
2014 December 2	2994.39	21:21:14	−2.3211	28 400	0.387
2014 December 2	2994.40	21:32:10	−2.3204	29 646	0.387
2014 December 3	2995.40	21:30:49	−2.2349	38 856	0.390
2014 December 3	2995.40	21:41:47	−2.2342	38 417	0.390
2014 December 19	3011.39	21:17:49	−0.8658	42 049	0.385
2014 December 19	3011.39	21:28:46	−0.8652	39 688	0.384
2014 December 21	3013.40	21:38:44	−0.6933	39 051	0.392
2014 December 21	3013.41	21:49:41	−0.6927	37 356	0.392
2015 January 6	3029.36	20:35:57	0.6728	39 935	0.390
2015 January 6	3029.37	20:46:56	0.6735	39 952	0.389
2015 January 10	3033.36	20:36:39	1.0153	41 780	0.384
2015 January 10	3033.37	20:47:36	1.0160	41 215	0.385
2015 January 17	3040.33	19:56:13	1.6122	31 182	0.380
2015 January 17	3040.34	20:07:11	1.6129	32 611	0.379

recovery of weak signatures in the line profile despite the presence of noise. The result is one high signal-to-noise ratio (S/N) spectral profile for each observation. To achieve this, a line list for a star with $T_{\rm eff} = 5000$ K, $\log g = 4.5$, a depth threshold of 0.1 and $\log({\rm M/H}) = 0.1$, and containing 12 220 lines was downloaded from the Vienna Atomic Line Database. This model atmosphere was used to generate a spectral weighting mask. This mask was applied to each observation (comprising a subset of four exposures with different polarimeter angles) with a step size of 1.8 km s^{-1}, matching NARVAL's detector pixel resolution. The resulting Stokes V profiles, which when convolved with the model line profile best matches the observed spectrum of the target star, are shown in the outer panels of Fig. 1. To parametrize the amount of emission in the Ca II H&K

Table 2. Stellar parameters.

Parameter	Value	Reference
Magnitude	$V = 3.7$	
Spectral type	K2V	Valenti & Fischer (2005)
Distance	3.2 pc	van Leeuwen (2007)
Effective temperature	5146 ± 31 K	Valenti & Fischer (2005)
Mass ($M_\odot$)	$0.856^{+0.006}_{-0.008}$	Valenti & Fischer (2005)
Radius ($R_\odot$)	0.74 ± 0.01	Baines & Armstrong (2012)
$v \sin i$ (km s^{-1})	$2.2^{+0.04}_{-0.04}$	Brewer et al. (2016)
$P_{\rm rot}$ (d)	11.68	Donahue, Saar & Baliunas (1996)
Inclination	$46^\circ \pm 2$	Jeffers et al. (2014)
Age	440 Myr	Barnes (2007)

values, we use an S-index calculated as described in Jeffers et al. (2014), where the S-index values calculated using NARVAL spectra are calibrated to the values from the Mount Wilson S-index survey by Marsden et al. (2014).

3 LARGE-SCALE MAGNETIC FIELD GEOMETRY

The large-scale magnetic field geometry is reconstructed using the tomographic technique of Zeeman–Doppler imaging (ZDI), which incorporates the maximum entropy algorithm described by Skilling & Bryan (1984). This method uses the stellar parameters shown in Table 2 to model local Stokes V profiles sampled over the stellar surface from which a disc integrated synthetic Stokes V profile is computed. This is then used to iteratively fit the model Stokes V profiles to the observed Stokes V profiles. The tomographic images of the large-scale magnetic field topology of ϵ Eridani are reconstructed by assuming that the field geometry is projected on to a spherical harmonics frame (Donati et al. 2006), where the magnetic energy is decomposed into poloidal and toroidal components. A spherical harmonics expansion with $\ell_{\rm max} = 10$ was used as there was no improvement to the fits using larger values. A reduced χ^2 of 1.05 was obtained for all of the maps when differential rotation was included in the image-reconstruction process.

3.1 Magnetic maps

The reconstructed large-scale magnetic field is shown in the central panels of Fig. 1. The observed and the modelled Stokes V LSD profiles are shown on the sides of the magnetic maps. Over the 5 month time-span of the observations, there is a significant evolution of the large-scale magnetic field topology of ϵ Eridani. The total observations were divided up into three epochs to avoid the presence of large gaps without observations, resulting from poor weather conditions. The division of the observations into the maps was tested for different combinations of observations (e.g. five maps versus three maps), and the result was comparable to the maps presented in Fig. 1, though a slightly lower χ^2 was obtained for the data set divided into three maps. We extensively tested the phase coverage of the maps by assigning random phases to the epochs of observation, which resulted in a very similar configuration of magnetic features. We determine the differential rotation of the magnetic features, as described in Jeffers et al. (2014), using the first two epochs, which was calculated to be $\Omega_{\rm eq} = 0.593$ rad d^{-1}, $\delta\Omega = 0.151$ rad d^{-1}, which is equivalent to $P_{\rm eq} = 10.58$ d and $P_{\rm pole} = 14.21$ d. This is in agreement with our previous measurements of differential rotation for ϵ Eridani using magnetic features (Jeffers et al. 2014). Other

differential rotation measurements for ϵ Eridani have been measured using photometric data taken with the *MOST* satellite, where values of 11.35 and 11.55 d are measured for two different spots (Croll et al. 2006), or $P_{\rm min} = 11.04$ d and $P_{\rm max} = 12.18$ d by Donahue et al. (1996). While all of these values broadly agree, the differences can be explained by each method measuring different features, for example, plage regions, photometry and magnetic features, which do not necessarily probe the same depth in the stellar atmosphere or stellar latitudes. Since there are a range of $v \sin i$ values in the literature, we also reconstructed the ZDI maps for an inclination of 30° corresponding to the lowest $v \sin i$ value of 1.7 ± 0.3 km s^{-1} (Saar & Osten 1997). To fit the Stokes V profiles required a higher χ^2 value to fit the images (1.12 compared to 0.99 for map 1). In the reconstructed maps, high-latitude features are slightly less extended in latitude and longitude, though not more than 5°–10°, for the radial component. The meridional and azimuthal components show a slight increase in the strength of the features of the order of 10 per cent. We conclude that the use of a lower inclination does not have any significant impact on the reconstructed features in the ZDI maps.

Even though the phase coverage of the last map is not optimal, we note that there is significant evolution of the Stokes V profiles between the same rotation phase (phase 0.67), which can be taken into account when differential rotation is included in the reconstruction of the maps. Additionally, for map 3, we note that the Stokes V profiles have the largest amplitudes and that a simple magnetic field topology is expected.

3.1.1 Radial component

The radial component of ϵ Eridani's large-scale magnetic field is dominated by a persistent and large polar magnetic spot of positive polarity, which varies in strength and shape. The strength of the region is highest in 2014.98 (map 3), and weakest in 2014.84 (map 2), while the global shape ranges in latitude from 30° (2014.84) to 60° (2014.98). The strongest evolution of the magnetic field is from epoch 2014.84 (map 2) to epoch 2014.98 (map 3), where the polar spot has increased in strength and evolved into a large spot, which is no longer centred at the pole and extends to much lower latitudes. This evolution of magnetic features is also evident in the corresponding Stokes V profiles. Additionally, there are weaker magnetic spots with negative polarity that are likely to be evolving from one epoch to the next. The strength of the negative regions is highest at epochs 2014.98 (map 3) and 2014.71 (map 1) and very weak at 2014.84 (map 2).

3.1.2 Azimuthal component

The azimuthal component of ϵ Eridani's large-scale field appears only very weakly with small hints of magnetic spots at epochs 2014.71 (map 1) and 2014.98 (map 3). The azimuthal field is strongest at epoch 2014.84 (map 2), where a large magnetic spot of negative polarity extends from phases 0 to 0.3.

3.1.3 Meridional component

The determination of the meridional field is often difficult due to the crosstalk between the meridional and the radial fields. As discussed by Donati & Brown (1997), the crosstalk between the radial and meridional fields primarily affects magnetic features at low latitudes, which implies that the higher latitude features are reliably reconstructed. This is evident in the magnetic maps, where the reconstructed negative polarity magnetic features at latitudes 0°–50° in the meridional field maps are mirrored in the radial field maps (for all maps). The presence of high-latitude meridional field in map 2 at phase 0.5 is considered to be reliable. An additional important consideration is whether the crosstalk is from radial to meridional or vice versa. As discussed by Donati & Brown (1997), for stars with low inclinations ($i < 30°$), the crosstalk is from radial to meridional, while for higher inclinations ($i > 50°$), the crosstalk will be from meridional to radial. Since the adopted inclination of ϵ Eridani is 46°, it lies between these two possibilities, and it is not possible to conclude in which direction the crosstalk occurs.

3.2 Magnetic energy

Over a period of approximately 5 months, ϵ Eridani's large-scale field evolves (as shown in Fig. 2 and Table 3) with decreasing S-index. The most dramatic changes are seen in the rapid emergence of an axisymmetric toroidal field. This is indicated by the colour of the points in Fig. 2 changing from red at 2014.71 (map 1) to green at 2014.98 (map 3). The field is notably more complex than a simple dipole at all epochs with significant amounts of the magnetic energy being contained in higher order modes. The poloidal component is approximately 50 per cent dipolar (with values ranging from 43 per cent at 2014.71 to 56 per cent at 2014.84), with additional contributions from the quadrupolar (with an average of 20 per cent) and octupolar components (which are typically of the order of 20 per cent) and higher order modes $l > 3$. The axisymmetry of the large-scale field is quite constant with an average value of 35 per cent.

4 DISCUSSION

The large-scale magnetic field geometry of ϵ Eridani has been shown to be highly variable over its 2.95 yr chromospheric activity cycle when observed at yearly epochs (Jeffers et al. 2014). To investigate the evolution on shorter time-scales of the magnetic field geometry of ϵ Eridani, we secured observations over a period of five successive months, from 2014 September to 2015 January, spanning ϵ Eridani's chromospheric activity minimum. The large-scale magnetic field is shown to vary on a time-scale of months with the first magnetic map reconstructed for epoch 2014.68 (map 1) showing significant evolution compared to the final map reconstructed for epoch 2014.98 (map 3). The large-scale magnetic field geometry is predominantly poloidal (ranging from 74 per cent to 84 per cent) throughout ϵ Eridani's activity minimum and in contrast to the rest of its activity cycle where it is also seen to have a strong toroidal component (Jeffers et al. 2014). The poloidal field is not a simple dipole but is quite complex with significant fractions in higher order modes such as quadrupolar and octupolar modes.

The reconstructed complex poloidal field is in contrast to the Sun, where its large-scale field is a simple dipole at activity minimum and becomes complex at activity maximum (DeRosa et al. 2012). On the Sun, the dipolar and quadrupolar modes vary in antiphase, such that after cycle minimum, the quadrupolar mode grows as the number of spots increases, reaching a maximum at cycle maximum (DeRosa et al. 2012). However, on ϵ Eridani, we observe a slight decrease in the quadrupolar mode at this phase, accompanied by a slight growth in the dipole mode. The changes are small, and a longer term study is needed to confirm if this is indeed the pattern that characterizes the cycle. The most significant change in ϵ Eridani's large-scale magnetic field is in the toroidal component of the axisymmetric field, which evolves from 5 per cent to 72 per cent precisely at the emergence of ϵ Eridani from its

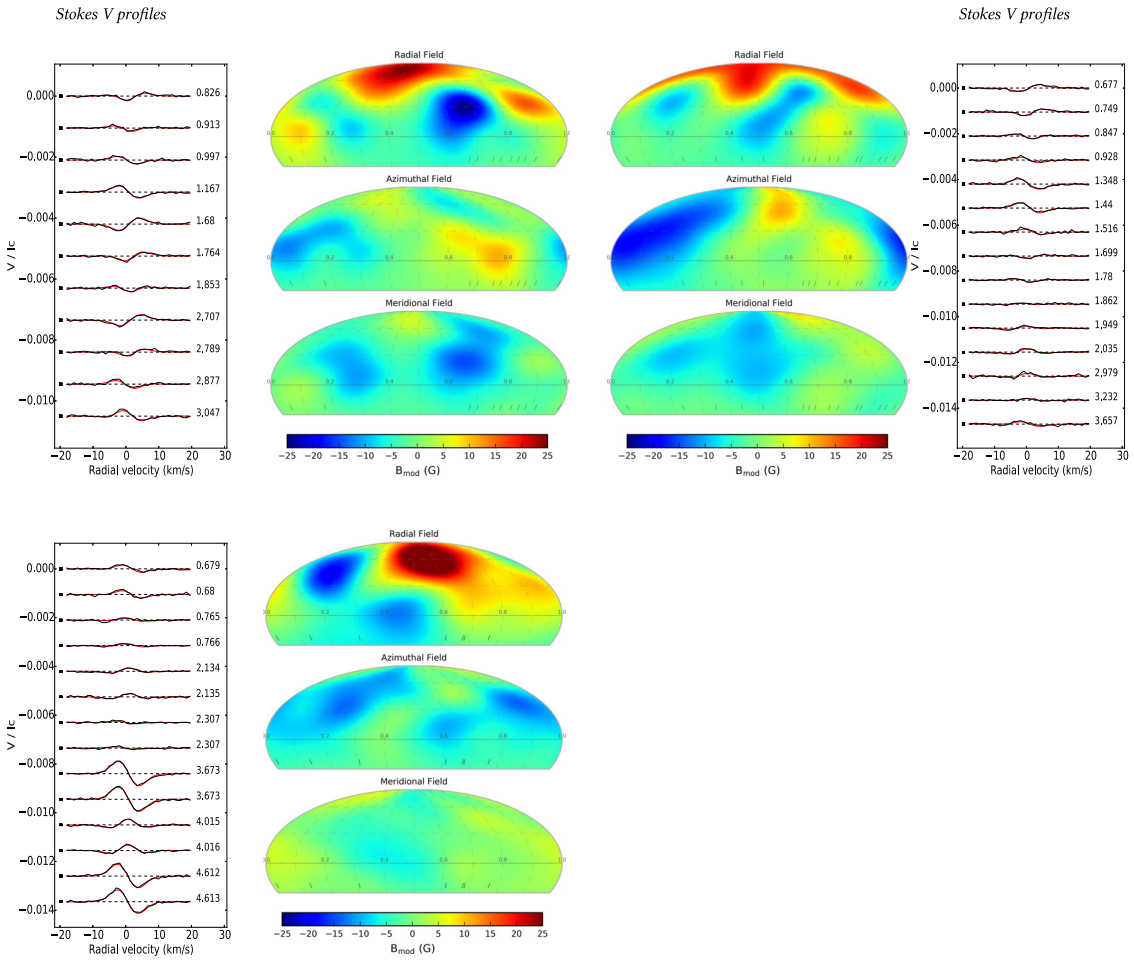

Figure 1. Magnetic field maps of ϵ Eridani reconstructed for 2014.71, 2014.84 and 2014.98, shown with the Stokes *V* fits to the sides (ordered from the left- to right-hand panel and top to bottom panel). For each image, the magnetic field projection is shown in terms of radial (upper panel), azimuthal (middle panel) and meridional (lower panel) field components, where red indicates positive polarity and blue indicates negative polarity. The magnetic field strength is in Gauss, where for each map the scale is identical ($B_{\rm max} = 25$ G). The tick marks at the top of each radial field map indicate the observational phases used to reconstruct the large-scale magnetic field geometry. The Stokes *V* profiles are plotted separated by a constant value for clarity.

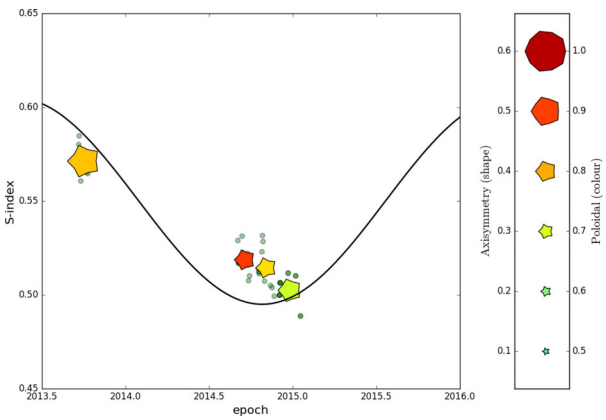

Figure 2. The evolution of ϵ Eridani's large-scale field during S-index minimum. The symbol shape indicates the axisymmetry of the field (non-axisymmetric by pointed star shape and axisymmetric by decagon), the colour of the symbol indicates the proportion of poloidal (red) and toroidal (blue) components of the field, and the symbol size indicates the magnetic field strength. Additionally, S-index points before and after the activity minimum are included (from Jeffers et al. 2014 and unpublished data). The black line indicates the sinusoidal period of 2.95 d and epoch of S-index minimum using the values of Metcalfe et al. (2013).

activity minimum and shows a strong axisymmetry, just like the Sun's poloidal field. Currently, there is limited information on the long-term evolution of the Sun's toroidal field as only a few years of vector data are available (Gosain et al. 2013; Vidotto 2016). Within this small time window, however, the solar toroidal field was much weaker than on ϵ Eridani. A longer term comparison of the variation of the toroidal field over the stellar magnetic cycle may shed some light on the nature of the magnetic cycle.

Another star that has been monitored as part of the BCool survey and that has stellar parameters very similar to ϵ Eridani is 61 Cyg A (Boro Saikia et al. 2016), which also exhibits a solar-like magnetic cycle. At activity minimum, the large-scale field of 61 Cyg A is also a simple dipole like the solar case, showing that it is not a limitation of ZDI that we do not see a similar behaviour for ϵ Eridani. The poloidal field of ϵ Eridani is more complex at activity minimum compared to 61 Cyg A and the Sun. The S-index cycle of 61 Cyg A is 7.2 $\pm$ 1.3 yr long (Boro Saikia et al. 2016), and its stellar parameters are more similar to ϵ Eridani than the Sun's. The mass of 61 Cyg A is 0.66 $M_\odot$ (Kervella et al. 2008), which is slightly smaller than ϵ Eridani's mass of 0.7 $M_\odot$, and given their low $v \sin i$ values, the ZDI technique has a similar resolving power for both stars. The evolutionary state of the two stars is similar to ϵ Eridani having an age that is approximately 7 per cent of its main-sequence

Table 3. The fraction of the large-scale magnetic energy reconstructed in the toroidal and poloidal field components; the fraction of the poloidal field in the dipolar ($\ell = 1$), quadrupolar ($\ell = 2$) and octupolar ($\ell = 3$) components; and the fraction of the energy stored in the axisymmetric component ($m = 0$) (e.g. the fraction of the poloidal field that is axisymmetric and the fraction of the toroidal field that is axisymmetric.)

Epoch	$B_{\rm mean}$ (G)	$B_{\rm max}$ (G)	Toroidal (per cent tot)	Poloidal (per cent tot)	Dipolar (per cent pol)	Quadrupolar (per cent pol)	Octupolar (per cent pol)	$\ell > 3$ (per cent pol)	Axisymmetric (per cent tot)	Poloidal (per cent axi)	Toroidal (per cent axi)
2014.71	8 ± 1	28	16	84	43	25	19	13	35	41	5
2014.84	8 ± 1	20	23	77	56	14	14	16	32	28	43
2014.98	10 ± 1	33	26	74	50	19	22	9	40	29	72

lifetime compared to 14 per cent for 61 CygA (calculated using the stellar evolution models of Pols et al. 1998). The main difference is the rotation periods of the two stars, with 61 Cyg A having a rotation period that is approximately three times as long, 35.4 d compared to ϵ Eridani's 11.68 d.

The strength of the mean magnetic field remains constant, despite the changing field geometry. In contrast to this, the maximum strength varies from 20 to 33 G. Since this is the strength in the large-scale component, there are likely to be additional contributions from the small-scale component that remains undetected with techniques such as ZDI. Evidence for additional small-scale field is shown by magnetic field measurements using Stokes I (unpolarized) line broadening, which measures the strength of both the large-scale and the small-scale fields. These values are typically of the order of 127 G (Valenti et al. 1995) or 165 G (Rüedi et al. 1997). As found by previous authors, the large-scale field is of the order of 10 per cent of the total field. The maximum and mean magnetic field strengths measured at 2014.9 (map 3) are comparable to previous values reconstructed at activity minimum (Jeffers et al. 2014, epoch 2011.81). Additionally, at epoch 2011.81, the large-scale field geometry has a large magnetic spot with positive polarity, which is very similar to the map reconstructed in 2014.9 (map 3). The two maps have the same fraction of poloidal field (74 per cent for both maps), which has a much more complex structure at 2014.9 compared to that at 2011.81. The main difference between the two maps is the fraction of axisymmetric field, which for epoch 2014.9 comprises 40 per cent and for epoch 2011.81 comprises 63 per cent. However, over the three epochs of this analysis, there are dramatic changes in the geometry of the axisymmetric field, which evolves from 41 per cent to 29 per cent for the poloidal component and from 5 per cent to 72 per cent for the toroidal component.

5 CONCLUSIONS

The high-cadence observations of ϵ Eridani's large-scale magnetic field geometry show that the large-scale magnetic field geometry evolves on a time-scale of months with a dramatic increase in the toroidal component of the axisymmetric field at the emergence from its activity minimum. The large-scale field also shows a predominantly poloidal component that is surprisingly complex when compared to the Sun at activity minimum. Our results show that the magnetic field of solar-type stars can be quite different from the Sun's even when they exhibit clear chromospheric activity cycles.

ACKNOWLEDGEMENTS

We would like to thank B. Carter, C. Folsom and V. See for valuable contributions in discussing the results of this Letter, and G. Anglada Escude and A. Reiners for their contributions to the observing proposal. JRB was supported by the UK Science and Technology Facilities Council (STFC) under the grant ST/L000776/1. SVJ was supported by Deutsche Forschungsgemeinschaft (DFG) Forschergruppe FOR 2544. The research leading to these results has received funding from the European Community's Seventh Framework Programme (FP7/2013-2016) under grant agreement number 312430 (OPTICON). This study was based on observations made through OPTICON with Telescope Bernard Lyot (TBL, Pic du Midi, France) of the Observatoire Midi-Pyrenees, which is operated by the Institut National des Sciences de l'Univers of the Centre National de la Recherche Scientifique (CNRS) of France.

REFERENCES

Aurière M., 2003, in Arnaud J., Meunier N., eds, EAS Publications Series Vol. 9, Magnetism and Activity of the Sun and Stars, EAS Publications Series. Toulouse, France, p. 105
Baines E. K., Armstrong J. T., 2012, ApJ, 744, 138
Barnes S. A., 2007, A&A, 669, 1167
Boro Saikia S. et al., 2016, A&A, 594, A29
Brewer J. M., Fischer D. A., Valenti J. A., Piskunov N., 2016, ApJ, 225, 32
Croll B. et al., 2006, ApJ, 648, 607
DeRosa M. L., Brun A. S., Hoeksema J. T., 2012, ApJ, 757, 96
Donahue R. A., Saar S. H., Baliunas S. L., 1996, ApJ, 466, 384
Donati J.-F., Brown S. F., 1997, A&A, 326, 1135
Donati J.-F., Semel M., Carter B. D., Rees D. E., Collier Cameron A., 1997, MNRAS, 291, 658
Donati J. -F. et al., 2006, MNRAS, 370, 629
Gosain S., Pevtsov A. A., Rudenko G. V., Anfinogentov S. A., 2013, ApJ, 772, 52
Jeffers S. V., Barnes J. R., Jones H. R. A., Reiners A., Pinfield D. J., Marsden S. C., 2014, MNRAS, 438, 2717
Kervella P. et al., 2008, A&A, 488, 667
Marsden S. C. et al., 2014, MNRAS, 444, 3517
Metcalfe T. S. et al., 2013, ApJ, 763, L26
Pols O. R., Schröder K.-P., Hurley J. R., Tout C. A., Eggleton P. P., 1998, MNRAS, 298, 525
Rüedi I., Solanki S. K., Mathys G., Saar S. H., 1997, A&A, 318, 429
Saar S. H., Osten R. A., 1997, MNRAS, 284, 803
Skilling J., Bryan R. K., 1984, MNRAS, 211, 111
Valenti J. A., Fischer D. A., 2005, ApJ, 159, 141
Valenti J. A., Marcy G. W., Basri G., 1995, ApJ, 439, 939
van Leeuwen F., 2007, A&A, 474, 653
Vidotto A. A., 2016, MNRAS, 459, 1533

This paper has been typeset from a TEX/LATEX file prepared by the author.